JOURNAL OF THERMOPHYSICS AND HEAT TRANSFER
Vol. 10, No. 2, April–June 1996

Assessment of Turbulence and Chemistry Models for Film-Cooled Nozzle Flows

R.-J. Yang*
National Cheng Kung University, Tainan 701, Taiwan, Republic of China

Systematic computation studies are conducted to show which physical effects are important and what physical models are required in high-speed film-cooled nozzle flows. Compressibility effects in turbulence models must be accounted for if shear layer spreading and wall heat fluxes are to be correctly predicted. Real gas effects are also quite significant, particularly as they account for widely varying thermochemical property variation because of large static temperature changes typical of nozzle flows.

Nomenclature

C_p = specific heat, J/kg-K
D = diffusion coefficient of mixture, m^2/s
D_{ij} = binary diffusion coefficient of i with respect to j, m^2/s
E_a = activation energy, J/kg-mole
g = Gibbs free energy, J/kg
h = enthalpy, J/kg
k = turbulent kinetic energy
k_m = thermal conductivity of mixture, kg/m-s
L_{ref} = reference length, 2.54 cm
M = Mach number
P_{ref} = reference pressure, 153 atm
p = static pressure, atm
Q_{ref} = reference heat flux, 11.36 kJ/m**2-s
R = gas constant, J/kg-K
T = static temperature, K
T_{ref} = reference temperature, 3726 K
x, y = Cartesian coordinates, m
y^+ = dimensionless normal distance, $\rho u_\tau y/\mu$
ε = turbulent dissipation rate

Subscripts
i, j = species indices

Introduction

ADVANCED nozzles have been considered for Earth-to-orbit (ETO) and single-stage-to-orbit (SSTO) applications, both in advanced rocket engines and airbreathing engines [e.g., Space Transport Main Engine (STME) and National Aerospace Plane (NASP)]. These high-performance systems typically expose hardware to high heat flux environments making active cooling essential. Film cooling is a promising technique for the reduction of high heat fluxes.[1] The design of the film cooling uses either normal injection or discrete slot injection tangential to the nozzle surfaces. The injected coolants interact with the core flow and result in fluid mixing and chemical reaction. Furthermore, large static temperature variation in the nozzles results in a significant variation in gas properties, which have to be properly modeled. Analytical methods, such as computational fluid dynamics (CFD) techniques, to design efficiently the film-cooled nozzles, require further development and validation before they can be applied with a high degree of confidence.

Received Aug. 10, 1995; revision received Nov. 7, 1995; accepted for publication Nov. 8, 1995. Copyright © 1996 by the American Institute of Aeronautics and Astronautics, Inc. All rights reserved.

*Associate Professor, Department of Engineering Science. Senior Member AIAA.

Turbulent transport models have had success in predicting the mean features of many incompressible flows.[2] However, attempts to extend these models to supersonic flows have been less effective. This is particularly true for the case of mixing layer. The decrease in normalized mixing-layer growth rate as the convective Mach number increases is not predicted by the incompressible turbulent models. The mixing-layer type of shear layer is one of the typical flows in film-cooled nozzle flows. The spreading rate has to be computed correctly to calculate correct heat fluxes at the wall. Sarkar et al.[3] and Zeman[4] proposed models to account for the compressibility effects. Viegas and Rubesin[5] use a k-ε two-equation model to assess these models in high-speed shear layers consisting of the same gas species. They showed the reduction in the shear-layer spreading rate with the compressibility correction included in the k-ε model. Since the considered film-cooled nozzle flow consists of different gas species, further assessment of the compressibility effect in the high-speed flow is still required.

High-speed film-cooled nozzle flows may encounter chemical reactions.[6] The thermodynamic property of the flow depends on the composition of the gas species. Widely varying static temperature affects the gas thermodynamic properties as well. Therefore, the chemistry models for the film-cooled flow should be evaluated. The choices of chemical model can interact with the numerical solution of the fluid dynamics problem. For cases where the characteristic fluid dynamics times are orders of magnitude different than the characteristic finite rate chemical times, the system becomes stiff and the selection of suitable time step sizes for each chemistry model can present problems. If the chemical times for a given problem are very small compared to fluid dynamics, one can assume local equilibrium. If the chemical times are long compared to the flow convection time, one must apply the frozen flow. If the chemical times are comparable to the flow times, one should employ a finite rate chemistry model. No document has been reported in the literature to compare perfect gas flow, frozen flow, and finite rate chemistry flow calculations for film-cooled nozzle flows. It is therefore interesting to perform calculations and to evaluate the flow behavior using the three different models.

In this study, we apply and modify a CFD code[7,8] to assess the effect of turbulence and chemistry models for the film-cooled nozzle flow. For completeness, the governing equations, physical modeling, and numerical procedure are briefly summarized. Finally, computed results are discussed and followed by a concluding remark.

Governing Equations

The two-dimensional, Navier–Stokes, and species continu-

ity equations for multiple species undergoing chemical reaction are stated in conservative form:

$$\frac{\partial Q}{\partial t} + \frac{\partial}{\partial x}(F_1 + G_1) + \frac{\partial}{\partial y}(F_2 + G_2) = S \qquad (1)$$

where

$$Q = \begin{bmatrix} e \\ \rho \\ \rho u \\ \rho v \\ Y_i \end{bmatrix}, \quad F_1 = \begin{bmatrix} (e+p)u \\ \rho u \\ \rho u^2 + p \\ \rho uv \\ \rho u Y_i \end{bmatrix}, \quad F_2 = \begin{bmatrix} (e+p)v \\ \rho v \\ \rho uv \\ \rho v^2 + p \\ \rho v Y_i \end{bmatrix}$$

$$G_1 = \begin{bmatrix} -\bar{k}_m \dfrac{\partial T}{\partial x} - \displaystyle\sum_{i=1}^{N-1} \rho D(h_i - h_N) \frac{\partial Y_i}{\partial x} - u\tau_{xx} - v\tau_{xy} \\ 0 \\ -\tau_{xx} \\ -\tau_{xy} \\ -\rho D \dfrac{\partial Y_i}{\partial x} \end{bmatrix}$$

$$G_2 = \begin{bmatrix} -\bar{k}_m \dfrac{\partial T}{\partial Y} - \displaystyle\sum_{i=1}^{N-1} \rho D(h_i - h_N) \frac{\partial Y_i}{\partial y} - u\tau_{yx} - v\tau_{yy} \\ 0 \\ -\tau_{yx} \\ -\tau_{yy} \\ -\rho D \dfrac{\partial Y_i}{\partial y} \end{bmatrix}$$

$$S = \begin{bmatrix} 0 \\ 0 \\ 0 \\ 0 \\ w_i \end{bmatrix}, \quad i = 1, 2, \ldots, N-1$$

where

$$\tau_{xx} = 2\bar{\mu}_m \frac{\partial u}{\partial x} - \frac{2}{3}\bar{\mu}_m \left(\frac{\partial u}{\partial x} + \frac{\partial v}{\partial y}\right)$$

$$\tau_{yy} = 2\bar{\mu}_m \frac{\partial v}{\partial y} - \frac{2}{3}\bar{\mu}_m \left(\frac{\partial u}{\partial x} + \frac{\partial v}{\partial y}\right)$$

$$\tau_{xy} = \bar{\mu}_m \left(\frac{\partial u}{\partial y} + \frac{\partial v}{\partial x}\right) = \tau_{yx}, \qquad \bar{\mu}_m = \mu_{\text{laminar}} + \mu_{\text{turbulent}}$$

$$\bar{k}_m = k_{\text{laminar}} + k_{\text{turbulent}}, \qquad D = D_{\text{laminar}} + D_{\text{turbulent}}$$

All of the dependent variables are mass averaged. Here, e is the total energy per unit volume, ρ is the density, u and v are the velocity components, Y_i are the species mass fraction, p is the pressure, T is the absolute temperature, D is the mixture diffusivity and is related to the mixture viscosity through the Schmidt number, h is the species enthalpy, $\bar{\mu}_m$ and $\bar{k}_m$ are the mixture kinematic viscosity and thermal conductivity, respectively, and w_i is the species production rate.

Physical Modeling

Some physical modeling is required in the present study, namely, modeling for thermodynamic properties, chemistry, and turbulence. This modeling is briefly described:

Thermodynamic Properties

Following the approach of Drummond et al.,[9] the thermodynamic properties of gas species are modeled as follows:

1) The laminar viscosity and thermal conductivity are determined from Sutherland's law for the individual species together with Wilke's law for the mixture values. The turbulent thermal diffusivity is evaluated through assuming a constant turbulent Prandtl number $Pr_t = 0.9$. Similarly, a constant turbulent Schmidt number is assumed to give turbulent species diffusivity $Sc_t = 0.7$.

2) The species conservation equations contain D. A simple derivation is as follows: Nonuniformities on the composition because of flow convection and chemical source terms result in mass and energy flux. Velocity in the x direction of species i relative to the mass-averaged velocity u of the mixture is $\tilde{u}_i$. Neglecting mass diffusion because of thermal (Soret effect) and pressure gradient results in a set of simultaneous equations (Stefan–Maxwell equations) for $\tilde{u}_i$ in terms of D_{ij}, $i = 1, 2, \ldots, N$, $j = 1, 2, \ldots, N$. An $N \times N$ system of equations has to be solved for the $\tilde{u}_i$. We assume that all D_{ij} are equal to D and use Fick's law to compute $\tilde{u}_i$ without solving the system of equations.

3) The thermodynamics properties C_{pi} (specific heat) of each component of the mixture is given by a single fourth-order polynomial fit in temperature

$$C_{pi}/R_i = A_i + B_iT + C_iT^2 + D_iT^3 + E_iT^4 \qquad (2)$$

which integrate to give enthalpy

$$h_i = R_iT[A_i + (B_i/2)T + (C_i/3)T^2 + (D_i/4)T^3 + (E_i/5)T^4] + F_i \qquad (3)$$

where F_i is the enthalpy of formation of species i at the standard state. The Gibbs free energy of species i is

$$g_i/R_i = A_i(T - \ell n\ T) - [(B_i/2)T^2 - (C_i/6)T^3 - (D_i/12)T^4 - (E_i/20)T^5] + (F_i/R_i) - G_iT \qquad (4)$$

The coefficients A_i, B_i, C_i, D_i, E_i, F_i, and G_i may be obtained from McBride et al.[10] The Gibbs energy of reaction ΔG_R can then be calculated as the difference between the Gibbs energy of product and reactant species.

Chemistry Model

Finite rate chemical reaction of gaseous H_2/O_2 are modeled in this study with a seven-species, seven-reaction model. The rate of each reaction is described by the Arrhenius law, which describes the dependencies of the reaction rate on pressure, temperature, and chemical composition. The reactants and all rate coefficients are listed in Table 1. The corresponding Arrhenius rate coefficients are taken from Drummond et al.[9] After these rates have been determined, the production rate of each species can be found from the law of mass action, and the chemical source terms can be computed.

Table 1 Chemical reactions and rate constants[a]

ID	Reaction	Rate constant in m-kgmol-s unit		
		A	b	E_a
1	$H + OH + M = H_2O + M$	2.21E16	−2.0	0.0
2	$H + H + M = H_2 + M$	6.53E11	−1.0	0.0
3	$H_2 + O_2 = OH + OH$	1.70E10	0.0	2.016E8
4	$H + O_2 = OH + O$	1.42E11	0.0	6.866E7
5	$OH + H_2 = H_2O + H$	3.160E4	1.8	1.269E7
6	$O + H_2 = OH + O$	2.07E11	0.0	5.757E7
7	$OH + OH = H_2O + O$	5.50E10	0.0	2.930E7

Note: M is a typical third body.
[a]Rate = $AT^b \exp(-E_a/R_0T)$ and R_0 = universal gas constant = 8314 J/kgmol-K.

Turbulence Model

The conventional incompressible type of turbulence model has been unable to predict correct spreading rate of supersonic mixing layer. Sarkar et al.[3] has proposed a model that takes into account the compressibility effect on turbulence model, which is based on some theoretical justification, rather than strict empiricism. He argued that the turbulent dissipation rate can be decomposed into solenoid dissipation and the compressible dissipation. He used an asymptotic analysis to the compressible Navier–Stokes equations and proposed a correction term to the turbulent kinetic energy equation to account for the compressibility effects. Applying his model to the k-ε two-equation yields:

$$\frac{\partial \rho k}{\partial t} + \frac{\partial \rho U_j k}{\partial x_j} = \frac{\partial}{\partial x_j}\left[\left(\mu + \frac{\mu_t}{\sigma_k}\frac{\partial k}{\partial x_j}\right)\right] - \overline{\rho u_i' u_j'}\frac{\partial U_i}{\partial x_j} - \rho\varepsilon + E_k \tag{5}$$

$$\frac{\partial \rho \varepsilon}{\partial t} + \frac{\partial \rho U_j \varepsilon}{\partial x_j} = \frac{\partial}{\partial x_j}\left[\left(\mu + \frac{\mu_t}{\sigma_\varepsilon}\frac{\partial \varepsilon}{\partial x_j}\right)\right] - C_1 f_1 \frac{\varepsilon}{k}\overline{\rho u_i' u_j'}\frac{\partial U_i}{\partial x_j} - C_2 f_2 \rho \frac{\varepsilon^2}{k} \tag{6}$$

where $E_k = -\rho\varepsilon M_t^2$, $M_t^2 = 2k/\gamma RT$. Note that E_k is always negative, serving as a sink to account for the compressible dissipation in the turbulence kinetic energy equation. The C_1, C_2, f_1, and f_2 are adopted from the Lam and Bremhorst model[11] for low-Reynolds number correction near solid boundaries.

Solution Scheme and Algorithm

Numerical studies carried out in this study are based on the Rockwell Science Center USA (Unified Solution Algorithm) code.[7,8] This is a full Navier–Stokes solver based on a finite volume approach. It employs a highly accurate total variation diminishing (TVD) formulation and Roe's approximate Riemann solver to compute fluxes. The code solves the Navier–Stokes equations and an arbitrary number of species equations in conservation form. The code possesses a multizone structured grid bookkeeping capability that facilitates the treatment of complex geometries. More details about the scheme can be found in Refs. 7 and 8. Some benchmarking results for this scheme with finite rate chemistry are given by Palaniswamy et al.[8] for the supersonic combustion of hydrogen and air.

Results and Discussion

Supersonic Turbulent Mixing Layer

The physics of incompressible mixing layers have been studied extensively. However, additional study is required to understand the decrease in shear-layer spreading rate at high speeds. Following Sarkar's et al.[3] model, a supersonic turbulent mixing layer has been tested in the present study. Figure 1 shows the results from a particular set of conditions for the shear layer between two airstreams. The high-speed stream has a velocity of $U_1 = 2500$ m/s, whereas the low-speed stream has a velocity of $U_2 = 800$ m/s. The thermodynamic quantities in the two incident streams were equal and were prescribed as $T = 800$ K, $P = 1$ atm, and $\rho = 0.44$ kg/m^3. The freestream Mach numbers of the two streams are 4.41 and 1.41, respectively, and the convective Mach number is 1.5. We used the same computational domain (0.1 × 0.05 m) and grid points (201 × 51) as Sarkar and Lakshmanan.[12] The grid spacing is uniform and stretched in the cross-stream direction. This grid system was found to be sufficient to provide practically grid-independent results. For a numerically converged solution, the residual is reduced at least five orders of magnitude. Figure 1 shows the shear-layer growth rate along the streamwise direction. It shows good agreement with the results of Sarkar and Lakshmanan.[12] It should be noted that we used a k-ε two-equation model to evaluate turbulent eddy viscosity. However, Sarkar and Lakshmanan[12] used a second-order closure to evaluate Reynolds stresses. The shear-layer thickness is defined as the distance between the two points of the mean velocity profile where the normalized streamwise velocity $U^* = (U - U_2)/(U_1 - U_2)$ is, respectively, 0.1 and 0.9. Compared with the result predicted by the incompressible type of k-ε model, it clearly shows that the model predicts the dramatically reduced growth rate of the supersonic mixing layer.

Holden Film Cooling Flow

Holden's test case[13] no. 45, a two-dimensional film cooling experiment was selected to test further the effect of turbulence models and chemistry models. Figure 2a depicts the geometry and the flow features. The freestream airflow over a splitter plate with cooler helium injected tangentially below. Air and helium streams interact each other after the splitter plate and form a shear layer. The hotter air eventually hits on the wall and transfers heat to the surface. Therefore, the spreading rate

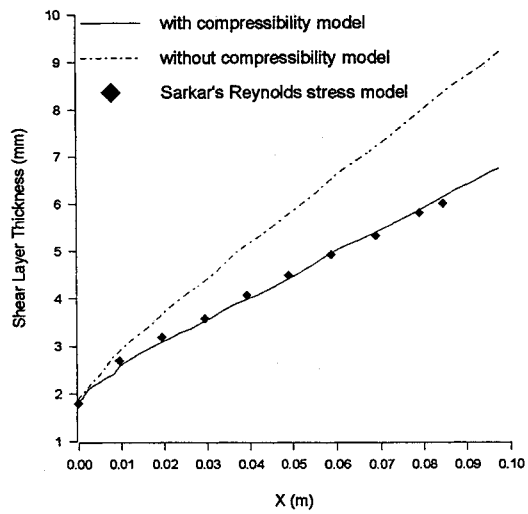

Fig. 1 Effect of compressibility on the growth of the shear-layer thickness along the streamwise direction.

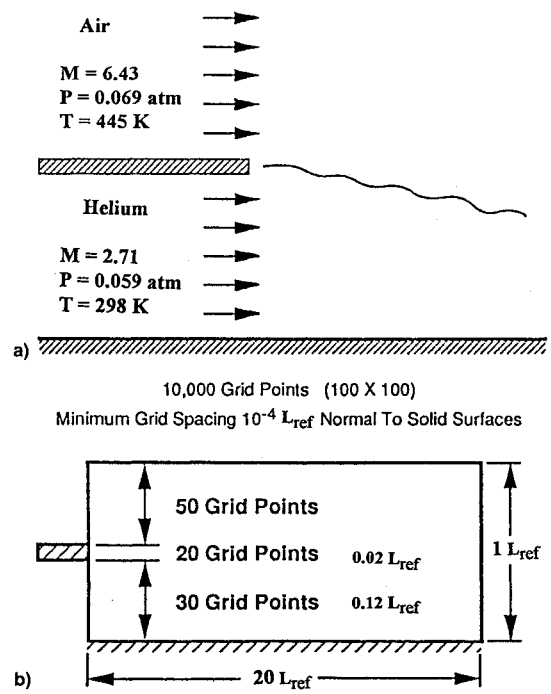

Fig. 2 a) Flow condition and b) grid points distribution of the Holden's film-cooling test case no. 45.

of the shear layer has to be predicted correctly to have good heat flux calculations. The compressibility effect on the spreading rate has been demonstrated previously. Air is treated as a real gas consisting of O_2 and N_2. No chemical reactions occur in this case since the air temperature (445 K) is below chemical reacting range. It should be noted that the real gas is defined as being thermally perfect gas, i.e., the air is treated as a mixture of perfect gases. The thermodynamic properties of each species are dependent on temperature. The computational grid point distribution is shown in Fig. 2b. We used 100 × 100 grid points with minimum grid spacing 10^{-4} of a L_{ref} normal to solid surfaces. The reference length is a unit inch. This makes the $y^+ < 1$ for this flow. The normal derivatives of species mass fractions are assumed to be zero along the wall surface. Figure 3 shows the computed heat flux distribution along downstream and its comparison with the experimental data. Results with compressibility effect included in the model have better agreement with the test data. This is justified by the fact that the shear-layer spreading rate is slower than that predicted by the model without including compressible dissipation. Therefore, the hot air hits the surface farther downstream, resulting in a smaller heat flux. Near the slot region, the heat transfer is dominated by the helium flow. This makes a similar agreement between the two models. The effect of compressibility is clearly shown to be significant for the heat transfer prediction.

Another calculation was performed in which air was treated as a single perfect gas component. The perfect gas is defined as being calorically perfect gas, i.e., constant thermodynamic properties. Both air and helium are regarded as perfect gases. The computed result is shown in Fig. 4. The real gas solution shows better agreement, particularly in the farther downstream regions. The major difference is caused by the variations of

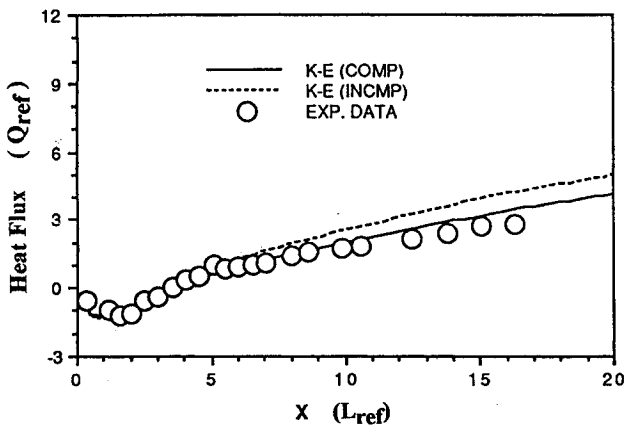

Fig. 3 Effect of compressibility in turbulence modeling on wall heat flux.

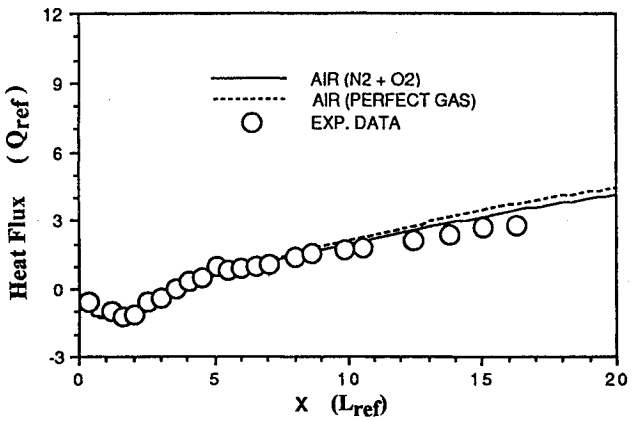

Fig. 4 Effect of chemistry model on wall heat flux.

Table 2 STME chamber flow conditions

Chamber conditions	Chamber gas compositions	
	Species	Mole fractions
Pressure, 153 atm	H	0.02977
Temperature, 3726 K	H_2	0.15003
Flow rate, 37.41 kg/s	H_2O	0.71975
Mach number, 0.213	O	0.00867
	OH	0.07520
	O_2	0.1642
	HO_2	0.00010
	H_2O_2	0.00005

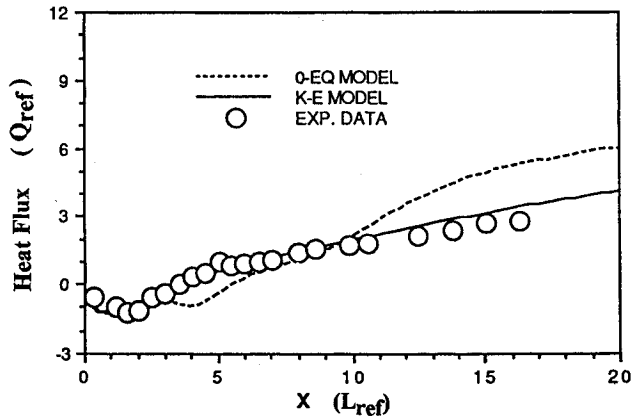

Fig. 5 Effect of turbulence model on wall heat flux.

thermodynamic properties mainly because of different gas compositions of the air. The temperature range of this flow is not wide enough to make a significant effect on the solutions shown in Fig. 4. However, for better simulation, the real gas effects should be included.

The algebraic turbulence model, the so-called zero-equation model, is frequently used in the CFD community. The key step in applying the model is to select adequate length scales for evaluating the turbulent eddy viscosity. The popular Baldwin–Lomax model[14] is used to simulate this flow together with the real gas model (air = O_2 + N_2). There are three distinct scales normal to the plate surface, namely, scales associated with boundary layer, potential core flow, and mixing layer, respectively. A simple geometry like this flow, however, makes the length scale selection difficult. A straightforward application of the Baldwin–Lomax model gives the result shown in Fig. 5. It clearly shows worse results than the two-equation model. The inconsistent result is because of the difficulty in selecting correct length scales and the compressibility effect in turbulence is not included in the zero-equation calculation.

STME Film-Cooled Nozzle Flow

The STME subscale nozzle[15] consists of three components: 1) a main combustion chamber, 2) an injector ring that constitutes the primary and secondary film coolant injectors, and 3) the nozzle wall. The flow conditions used in the simulation are shown in Table 2.

Hydrogen is used as the film coolant in the primary and secondary injectors. The primary injector injects the supersonic coolant parallel to the nozzle stream, and the secondary injector injects the subsonic coolant normal to the nozzle stream, as indicated in Fig. 6. The flow conditions for the primary injector are pressure 3.3 atm, temperature 210 K, flow rate 0.69 kg/s, and, Mach number 1.454. The secondary injector has the following flow conditions: pressure 4 atm, temperature 295 K, flow rate 0.12 kg/s, and Mach number 0.205.

For simplicity, the flow was assumed to be axisymmetric. A three-zone computational grid was developed for the flow calculation. The grid points for each zone are 80 × 41, 31 × 61,

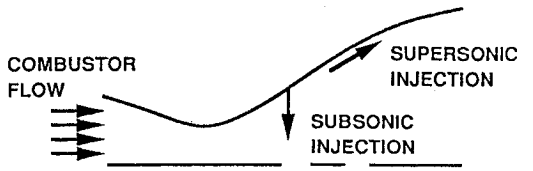

Fig. 6 STME film-cooled nozzle flowfield schematic.

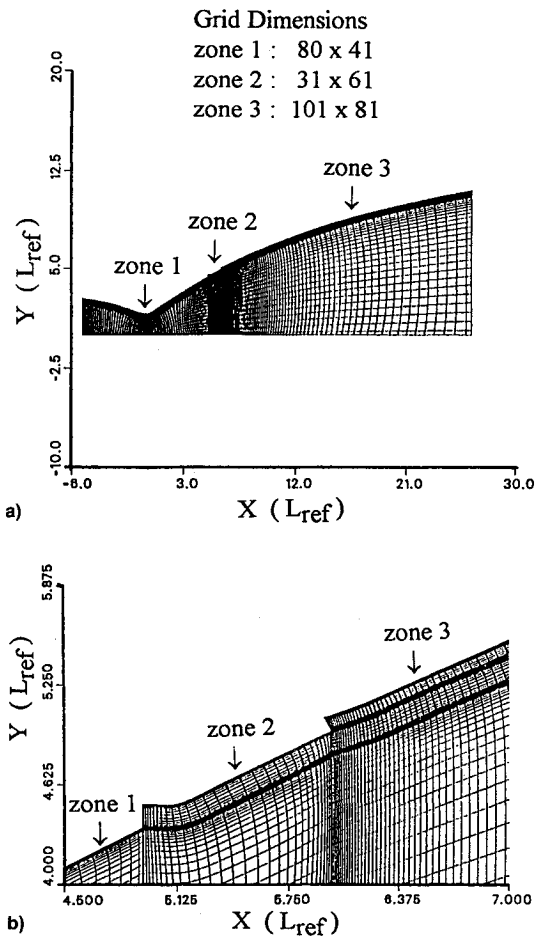

Fig. 7 a) Computational grid of the film-cooled nozzle flow and b) blown-up view near the injection region.

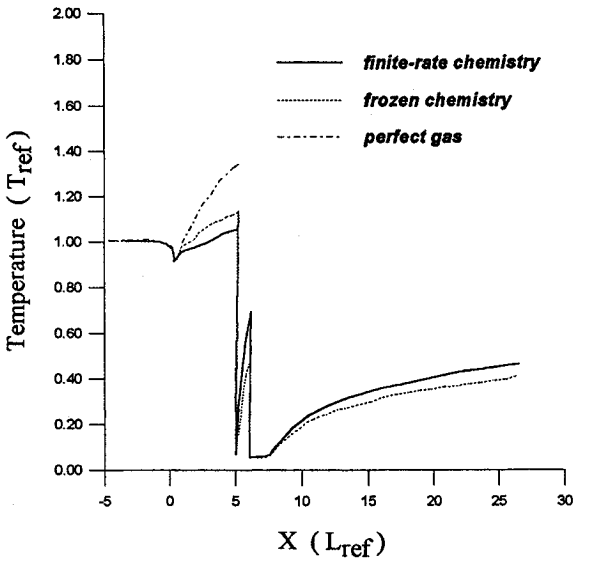

Fig. 8 STME nozzle surface temperature distribution.

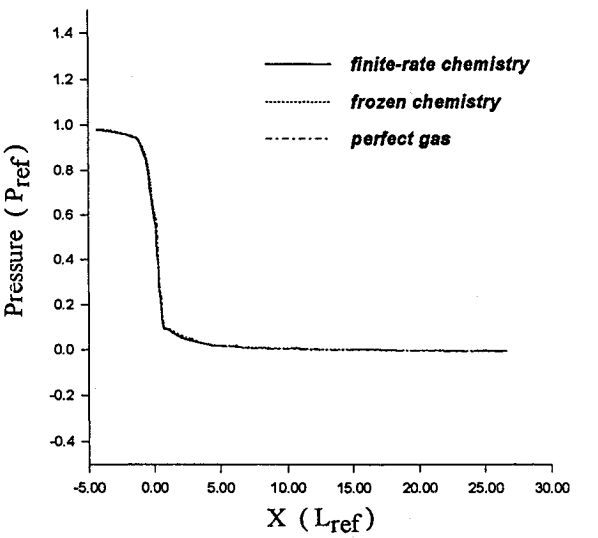

Fig. 9 STME nozzle surface pressure distribution.

and 101 × 81, respectively. The total meshes are 13,352. The grid lines were matched each other between zonal boundaries. The grid for each zone was generated by an elliptic solver. Grid lines are also clustered around the throat area, toward solid surfaces, and in the shear-layer region. Figure 7a shows the overall grid distribution. A close-up view for the zonal interface is shown in Fig. 7b.

The mole fraction of HO_2 and H_2O_2 are very small compared to the rest of the species. Therefore, these species were neglected and replaced by N_2 as inert gas. To understand the effect of chemistry models on the computed flow, three cases were studied: perfect gas, frozen chemistry, and finite rate chemistry. In the perfect gas assumption, the flow is assumed to have constant thermodynamic properties. In the frozen chemistry assumption, the flow is assumed to have real gas effects through mass diffusion, but no chemical reactions among species. The real gas of the frozen flow is defined as a nonreacting gas mixture of thermally perfect gases. In the finite rate chemistry model, the flow is assumed to have chemical reactions with seven mechanistic reaction steps. The reactants and all rate coefficients are listed in Table 1.

The flow is assumed to be fully turbulent and the k-ε two-equation model with the Sarkar's compressibility correction is applied to evaluate the turbulent eddy viscosity. Figure 8 shows the computed temperature distribution at the nozzle surface along the axial direction. In this computation, an adiabatic wall boundary condition was used. It shows that real gas effects are important in characterizing the thermal distributions. The throat is located at $x = 0$. Surface temperatures are almost identical to each other before the throat. After the throat the temperatures behave differently because of changes in thermodynamic properties. The H_2 coolant is injected normally to the nozzle surface at $x = 5$. Therefore, the surface temperature drops to the coolant temperature. Similarly, at $x = 6$, the H_2 is injected tangentially to the nozzle surface and the temperatures drop to the coolant temperature. Temperatures rise along the x direction because of high-speed viscous dissipation. The temperature distribution of the perfect gas model is not shown after the injecting ports because the coolant is not modeled in the calculation. Figure 9 shows the computed surface pressure distribution along the axial direction. Unlike the thermal field shown in Fig. 8, the pressure distributions are not as sensitive to the real gas effects as the temperature distributions.

These calculations were conducted on a Cray Y-MP machine. The CPU time per iterative step for each case was evaluated and given as 0.45 s for the perfect gas model, 1.6 s for the frozen gas model, and 2.3 s for the finite rate model, respectively. Nearly 3000 time steps are required to reduce the

residual five orders of magnitude. The CPU time for the perfect gas model is much less compared to the other cases because there are six-species equations less in the calculation. In the finite rate model, it requires 44% more CPU time compared to that of the frozen gas model.

Concluding Remarks

In the present study, some calculations have demonstrated the importance of turbulence and chemistry models in film-cooled-type flows. For the supersonic mixing-layer computation, compressibility effects in the turbulence model are required to be included for predicting a correct shear-layer spreading rate. Without including the effect, the shear layer spreads faster than the real condition and yields an inaccurate solution. For the Holden's film-cooling test case, a turbulent shear layer is formed between the injected film fluid and the external core flow. Effects of turbulence and chemistry models on the heat transfer rate at the wall surface are studied. Computed results are compared with experimental data. It again indicates the importance of including compressibility effects and the superior usage of the two-equation rather than the zero-equation turbulence modeling. Similar to the previous supersonic mixing layer, to compute correct shear-layer growth rate between the film fluid and the core flow requires the inclusion of compressibility effects in the turbulence model. The two-equation modeling gives an adequate evaluation for the eddy viscosity, in contrast to the difficulty of the zero-equation modeling in the selection of correct length scales. The effect of gas composition on the heat transfer for the air is also demonstrated. Real gas composition consisting of O_2 and N_2, instead of assuming an ideal single gas for air, predicts better experimental agreement. Finally, the STME film-cooled nozzle flow is computed together with three chemistry models for H_2/O_2, namely, perfect gas, frozen chemistry, and finite rate chemistry. Computed results indicate that the dependence on the choice of the chemistry models in the thermal field is more pronounced than in the pressure field.

Acknowledgments

This computational work was carried out at the Rocketdyne Division of Rockwell International. The author would like to thank S. Chakravarthy, D. Ota, U. Goldberg, and S. Palaniswamy of the Rockwell International Science Center for their helpful discussions during the course of this study.

References

[1]O'Connor, J. P., and Haji-Sheikh, A., "Numerical Study of Film Cooling in Supersonic Flow," *AIAA Journal*, Vol. 30, No. 10, 1992, pp. 2426–2433.

[2]Wilcox, D. C., "Turbulence Modeling for CFD," DCW Industries, Inc., La Cañada, CA, 1993.

[3]Sarkar, S., Erlebacher, G., Hussaini, M. Y., and Kreiss, H. O., "The Analysis and Modeling of Dilatational Terms in Compressible Turbulence," *Journal of Fluid Mechanics*, Vol. 227, 1991, pp. 473–493.

[4]Zeman, O., "Dilatation Dissipation: The Concept and Application in Modeling Compressible Mixing Layers," *Physics of Fluids A*, Vol. 2, No. 2, 1990, pp. 178–188.

[5]Viegas, J. R., and Rubesin, M. W., "Assessment of Compressibility Corrections to the k-ε Model in High-Speed Shear Layers," *AIAA Journal*, Vol. 30, No. 10, 1992, pp. 2369, 2370.

[6]Kim, S. C., and VanOverbeke, T. J., "Performance and Flow Caculations for a Gaseous H_2/O_2 Thruster," *Journal of Spacecraft and Rockets*, Vol. 28, No. 4, 1991, pp. 433–438.

[7]Chakravarthy, S. R., Szema, K.-Y., and Haney, J. W., "Unified Nose-to-Tail Computation Method for Hypersonic Vehicle Applications," AIAA Paper 88-2564, June 1988.

[8]Palaniswamy, S., Chakravarthy, S. R., and Ota, D. K., "Finite Rate Chemistry for USA-Series Codes: Formulation and Applications," AIAA Paper 89-0200, Jan. 1989.

[9]Drummond, J. P., Rogers, R. C., and Hussaini, M. Y., "A Numerical Model for Supersonic Reacting Mixing Layers," *Computer Methods in Applied Mechanics and Engineering*, Vol. 64, 1987, pp. 39–60.

[10]McBride, B. J., Heimel, S., Ehlers, J. G., and Gordon, S., "Thermodynamic Properties to 6000 K for 210 Substances Involving the First 18 Elements," NASA SP-3001, 1963.

[11]Lam, C. K. G., and Bremhorst, K. A., "Modified Form of k-ε Model for Predicting Wall Turbulence," *Journal of Fluids Engineering*, Vol. 103, Sept. 1981, pp. 456–460.

[12]Sarkar, S., and Lakshmanan, B., "Application of a Reynolds Stress Turbulence Model to the Compressible Shear Layer," *AIAA Journal*, Vol. 29, No. 5, 1991, pp. 743–749.

[13]Holden, M. S., "A Data Base of Experimental Studies of Shock Wave/Wall Jet Interaction in Hypersonic Flow," Calspan—Univ. at Buffalo Research Center, Buffalo, NY, April 1990.

[14]Baldwin, B. S., and Lomax, H., "Thin-Layer Approximation and Algebraic Model for Separated Turbulent Flows," AIAA Paper 78-257, Jan. 1978.

[15]Yang, R.-J., "Technology Test Bed Engine CFD Combustion Devices Consortium: STME Nozzle Design and Analysis Study," Contract Rept., NASA/MSFC, NSA8-40000, RSS-8869-15, 1992.